Article:
Grosse, Philipp, Gembus, Jan Luca, Landwehr, Felix et al. (2025) In-Liquid Plasma Catalysis for Nitrogen Reduction. ACS Energy Letters. pp. 378-388. ISSN: 2380-8195

https://doi.org/10.1021/acsenergylett.5c01740

ACS Energy LETTERS

Open Access

http://pubs.acs.org/journal/aelccp

Letter

In-Liquid Plasma Catalysis for Nitrogen Reduction

Philipp Grosse,* Jan-Luca Gembus, Felix Landwehr, Alex Ricardo Silva Olaya, Daniel Escalera-López, Nikita Bibinov, Andrew Robert Gibson, Sebastian Zeki Oener, and Beatriz Roldan Cuenya*

Cite This: ACS Energy Lett. 2026, 11, 378−388

Read Online

ACCESS | Metrics & More | Article Recommendations | Supporting Information

ABSTRACT: Ammonia, a crucial component in fertilizers and fuels, is currently produced by the energy-intensive Haber-Bosch process. However, due to the high upfront investments required for large-scale centralized production, alternative routes for small-scale applications are being sought.

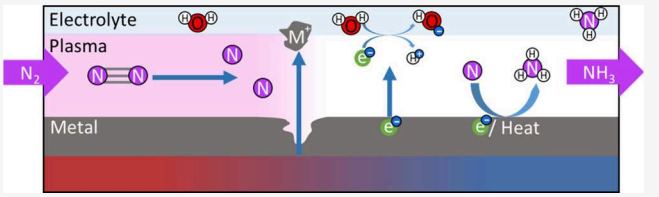

We integrate an in-liquid plasma discharge with electrocatalysis for ammonia generation from nitrogen and water in a single reactor. Among materials tested, platinum emerged as the most stable and active catalyst, it evolves hydrogen without plasma but produces significant ammonia under cold or hot in-liquid plasma. Our system employs a dual mechanism: plasma activates N_2, while the elevated Pt electrode temperature drives water decomposition (thermally and via plasma pathways), releasing reactive hydrogen. This synergy stabilizes key NH intermediates, enabling ammonia production beyond conventional electrocatalysis and eliminating the need for added hydrogen. Under optimized plasma conditions, partial current densities up to 3 mmol h^{-1} cm^{-2} at 250 mA cm^{-2} are achieved. Control measurements across various metals confirm a synergistic plasma-catalysis effect.

Ammonia (NH_3) production through the Haber−Bosch process has been a transformative achievement that enabled quadrupling global agricultural output and, thus, supporting a world population of over eight billion. Recently, ammonia has garnered attention as a potential green energy vector, where hydrogen produced from water electrolysis and renewable energies is used to generate green NH_3, which can then be thermally or electrochemically decomposed to release the green hydrogen on demand. However, the optimized Haber−Bosch process necessitates high operating temperatures (>400 °C) and pressures (>200 atm) and requires cost-intensive upfront investments for large-scale centralized production.[1,2] Additionally, the associated infrastructure requires substantial investments in H_2 feedstock generation, ammonia transportation, and storage.[3] Thus, small- to medium-sized, decentralized alternatives for ammonia production are highly sought after, especially the ones powered by renewable energy sources such as solar and wind for direct, on-demand NH_3 production.[4,5]

Electrochemical ammonia synthesis, directly from nitrogen (N_2) and water, holds promise for small-scale, environmentally sustainable ammonia production, with potential economic and social benefits, particularly in developing countries and remote areas lacking sufficient infrastructure.[1,6] Thus, the electrocatalytic nitrogen reduction reaction (NRR) has received interest as a promising avenue for small-scale NH_3 production. However, direct NRR faces intrinsic limitations due to the unreactive nature of triple-bonded N_2, its low solubility in water, and limited durability of nonaqueous electrolyte alternatives.[7,8]

Conversion of the stable N_2 into a more reactive intermediary form is a critical step during this process. For the electrocatalytic NRR, various strategies have been explored to activate the triple bond of N_2,[6,9−13] including lithium redox intermediates, transition metal catalysts, metal nitrides, and molecular catalyst systems.[8,12,14−17] Lithium-mediated pathways remain an important example, where the Li redox intermediate is thought to play a critical role in N_2 activation. Besides the electrocatalytic pathway, plasma has been also tested in various plasma conditions. Further, it has been recently postulated that inactive catalyst materials may be activated utilizing spin-mediated promotion by the addition of hetero metal atoms.[18,19] Alternatively, a pathway utilizing nitrite and nitrates (NO_3^- and NO_2^-) as highly soluble intermediates is under investigation.[14−16] NOx, derived from these species can be readily converted into NH_3.[17] However, industrially, nitrites and nitrates are typically produced from ammonia via the greenhouse gas intensive Ostwald process.[20] Historically, thermal plasma and arc furnaces were used for nitrogen fixation, which, in fact, predated the development of the Haber-Bosch process, but faced energy efficiency challenges.[21,22] The application of plasmas in combination with liquids has been explored in a range of laboratory-scale

Received: June 8, 2025
Revised: December 17, 2025
Accepted: December 19, 2025
Published: December 30, 2025

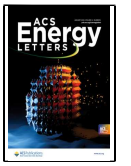

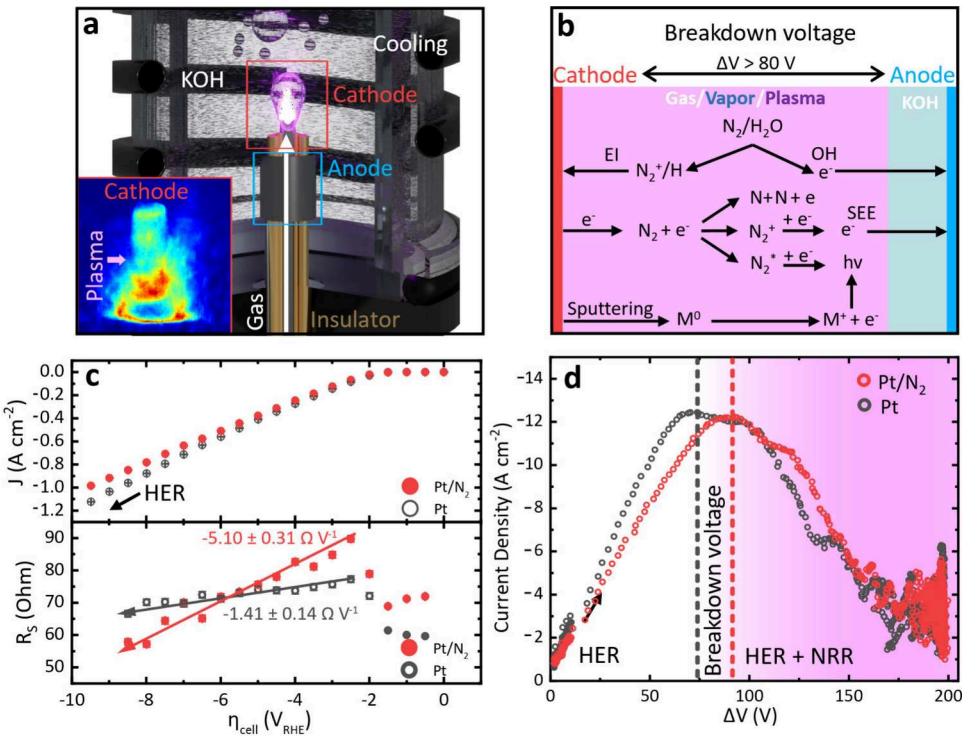

Figure 1. Setup and electrochemical performance. (a) Schematic representation of the reactor cell, with the cathode being enclosed within an insulating gas tube, and the Pt anode foil surrounding the external surface of the gas tube. 0.5−4.0 mm of the inner electrode is exposed to the electrolyte. Gas is evolving from the exposed area of the inner electrode and additionally, N_2 is injected from within the gas tube. (b) Schematic of relevant interfacial processes. The governing effects at the interface are the excitation-ionization (EI) of gas/vapor molecules, secondary electron emission (SEE) and radiative recombination. Sputtering is unlikely to occur at the applied voltages, but local hot spots in the plasma may eject metal atoms from the cathode. (c) Polarization curves of Pt acting as cathode material up to −10 V (top), with solution resistance (bottom). Current values are average values over 5 min chronoamperometry at each potential. Error bars represent standard deviation. The legend distinguishes experiments with Pt cathode under N_2 plasma (Pt/N_2) from those without N_2 flow (Pt, HER-only control). (d) Continuation of the diffusion-limited current−voltage curve as measured by the high-voltage probe, revealing a voltage breakdown and plasma ignition at approximately 80 V with 0.07 L min^{-1} N_2 gas flow and around 70 V without N_2.

configurations, including dielectric barrier discharges,[23,24] gliding arc plasmas,[25] plasma-over-liquid systems,[26−28] and plasma−liquid bubble reactors. These approaches have demonstrated that temperature,[29] discharge mode, and gas−liquid mass transfer strongly influence nitrogen activation in N_2/H_2O plasmas. However, plasma-over-liquid and bubble-based systems often operate without direct contact between the plasma and a solid electrode and therefore predominantly favor nitrogen oxidation pathways (NO_x formation), rather than sustained NH_3 synthesis.[23,30] In contrast, in-liquid electrode plasmas can introduce direct plasma−electrode coupling, which fundamentally alters the local reaction environment by modifying hydrogen availability and enabling surface-mediated stabilization of reactive nitrogen species.

Here, we report an in-liquid plasma approach to ammonia synthesis in aqueous media, in which a metal cathode operates within a submerged plasma discharge with the goal of overcoming the low current densities and NH_3 production rates typically reported for purely electrocatalytic nitrogen reduction reaction (NRR). The process couples plasma activation of N_2 and H_2O vapor with potential surface reactions on the heated cathode. We study the electrochemical response of our reactor and various electrode materials and feed conditions to identify and understand key parameters influencing the efficiency and kinetics of ammonia formation. Additionally, optical emission spectroscopy (OES) provides key insights into the plasma properties and ammonia production rates. In our approach, we harness not only the energetic activation of N_2 by the plasma, but also exploit the high temperature of the electrode to drive thermal (catalyzed) water decomposition. This produces a concentrated source of hydrogen radicals that, when combined with activated nitrogen species on the Pt surface, may form key intermediates (e.g., NH radicals), leading to efficient ammonia synthesis.

Finally, we discuss challenges and benefits of synthesizing ammonia from nitrogen (N_2) and water via this new pathway, keeping in mind that this is until now only a proof-of concept experiment and by no means a process that can in any way compete with the efficient Haber-Bosch process.

REACTOR DESIGN AND PLASMA IGNITION

Plasma-driven ammonia synthesis using water as the hydrogen source has recently been demonstrated by Sharma et al.[27] in a two-stage configuration where plasma activation and electrochemical reduction occur in physically separated compartments. Nonetheless, little is still known about the chemical processes taking place at the various interfaces involved, and further work is still needed to improve the efficiency. Other configurations, including gas-phase dielectric barrier discharges over aqueous cathodes[28] plasma−over−liquid (micro)-discharges,[27,31] gliding arc discharges,[25] and hybrid plasma−electrolysis cells[32] have been used as well. These plasma−water systems have demonstrated ammonia formation rates in the range of μmol h^{-1}, with energy efficiencies varying widely

https://doi.org/10.1021/acsenergylett.5c01740
ACS Energy Lett. 2026, 11, 378−388

depending on plasma power density, reactor design, and electrolyte composition. The present work describes an in-liquid plasma−electrolytic design integrating the former two functions into a single reactor, placing the catalyst directly in the plasma sheath. This configuration enables simultaneous exposure to plasma-activated nitrogen and hydrogen radicals generated thermally and by plasma pathways at the same interface, potentially enhancing coupling between the two processes. While the Sharma design offers the practical advantage of reduced electrode erosion and stable operation, it requires additional gas−liquid transfer steps between activated plasma species and the generated hydrogen that may diminish interfacial reaction efficiency. In contrast, our proof-of-concept approach prioritizes the in depth understanding of the interfacial processes taking place at the gas/liquid/solid plasma electrode interface and maximizing the plasma-catalyst coupling without the full physical separation of plasma and electrochemistry-related processes (see Figure 1a).

To combine a plasma with electrocatalysis, we designed a single compartment, two-electrode reactor comprised of a platinum (Pt) counter electrode (anode) and a working electrode (cathode) (Figure 1a, Supplementary Figure 1). A 1.0 mm diameter wire of variable length and material serves as active plasma and electrocatalytic working electrode (cathode). The wire is placed within a slightly larger inner diameter ceramic tube (alumina), which is exposed to a continuous N_2 gas flow. The counter electrode, consisting of a Pt-foil, surrounds the ceramic tube at a distance of approximately 5 mm from the working electrode. Additionally, an external circulating cooler is used to minimize the evaporation of the electrolyte (0.1 M KOH) and NH_3 outgassing during plasma operation. It was found that an alkaline pH (here 14) reduces the erosion of the plasma electrode. Various metal wires were tested as plasma electrodes. The selection was made based on their electrocatalytic properties in facilitating the hydrogen evolution reaction (HER), including Ni, Cu, Ir, and Pt. Additionally, Hf, Ti, Ta, Mo, and W, which are covered with amorphous or even nonconductive oxides under typical HER potentials, but become metallic at large negative potentials and were also tested. Figure 1a,b depict the reactor setup and the multiphase environment under operating conditions. When plasma is ignited, a gas/vapor sheath forms around the cathode, composed of N_2, H_2, and water vapor from HER and thermal decomposition. Optical emission spectroscopy and FE data indicate that NH_3 is produced predominantly at the plasma-electrolyte interface and directly on the Pt cathode surface, where plasma-activated nitrogen species interact with hydrogen radicals. The schematic in Figure 1b marks this NH_3 formation zone within the gas/vapor layer adjacent to the electrode.

With increasingly reducing potential, the HER in alkaline electrolyte ($2\ H_2O + 2\ e^- \leftrightarrow H_2 + 2\ OH^-$) starts to generate H_2. In combination with the nitrogen flow from the ceramic tube, a gas/vapor layer forms, which now comprises a mixture of nitrogen, hydrogen, and water vapor progressively enveloping the working electrode (cathode). At potentials exceeding 80 V, the gas/vapor sheath that forms around the cathode is not merely a barrier for charge transport; it becomes a reactive zone, where the elevated temperature and plasma trigger thermal decomposition of water. This process generates a rich supply of hydrogen radicals that should rapidly interact with atomic nitrogen and excited molecular nitrogen species, produced by electron impact in the plasma, to form NH radicals, the critical intermediates for ammonia synthesis. In this state, free electrons, which are produced by ionization of gas molecules, drift toward the gas/electrolyte interface. Positively charged ions, produced during the ionization process, impact on the cathode surface and cause secondary electron emission. Because of the low mobility of the heavy ions, the electric field near the cathode surface is high and secondary electrons can be accelerated strongly. The thickness of this so-called plasma sheath region, or "cathode fall", is typically several micrometers under atmospheric pressure conditions. Outside of the cathode fall, the electrons lose kinetic energy by elastic and inelastic collisions with neutral and charged species in the gas-phase plasma bulk region. In addition, free electrons can collide with charged species and neutral species, leading to a variety of outcomes, such as (radiative) electron-positive ion recombination, electron-attachment to neutral species, electron impact excitation of rotational, vibrational and electronic states of neutrals and ions, and electron impact dissociation of molecular species. The products of these reactions will also collide with one another, leading to a nonequilibrium gas-phase plasma chemistry. In addition, sputtering of metal atoms from the cathode may also occur. These sputtered atoms will also participate in the gas-phase chemistry described above. Some of these processes are shown schematically in Figure 1b.

Chronoamperometry and impedance spectroscopy (EIS), both with and without nitrogen flow were used to study the electrochemical behavior of the system (Figure 1c). At voltages below the plasma ignition threshold (~80 V), the system operates in a hydrogen evolution regime without detectable ammonia formation. Only when plasma ignition occurs, do we detect ammonia at rates far above the electrocatalytic baseline, indicating that plasma activation is essential for NH_3 formation in our reactor. This transition is shown in Figure 1c,d, where the change in current−voltage behavior coincides with the onset of ammonia generation around the breakdown voltage (80 V). The series resistance was extracted from the high-frequency impedance at each potential step. Figure 1d shows an exemplary polarization curve for Pt until voltage breakdown and plasma ignition at ~ 80 V with 0.07 L min^{-1} and without N_2 gas flow. All polarization curves and corresponding EIS for the different metal wires are shown in Supplementary Note 1. For all materials, no significant differences in current and resistance are apparent once the potential enters the diffusion-limited regime. The sole exception is Hf, which features a natural passivation layer that only gets removed under harsh plasma conditions. The introduction of nitrogen gas resulted in a decreased current and increased resistance, by covering parts of the electrode in N_2 gas until eventually a full vapor layer forms at higher potentials. The j vs V plots in Supplementary Figure 10 highlight differences between experiments conducted with and without nitrogen. These results indicate that the reactor is initially at low voltages mainly governed by HER, and no measurable NH_3 formation occurs with the tested materials.

Optical Emission Spectroscopy and Plasma Characterization

To probe the influence of the cathode material (Pt and W wires) on the conditions of the plasma in the system and subsequent catalytic performance, optical emission spectroscopy was used (Figure 2). These two metals showed stable plasma generation, but distinctly different NH_3 production

https://doi.org/10.1021/acsenergylett.5c01740
ACS Energy Lett. 2026, 11, 378−388

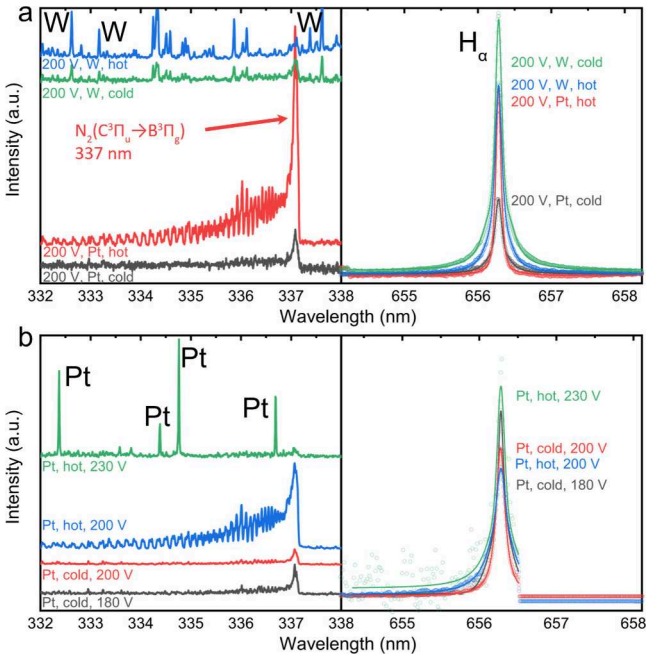

Figure 2. Plasma characterization. (a) OES data illustrating N_2(C−B,0−0) vibrational transitions and rotational bands as well as the H_α line for both, hot and cold plasma states for Pt and W cathodes. (b) N_2 transition with a Pt cathode is depicted across different applied voltages ranging from 180 to 230 V. Vibrational excitation and ionization of nitrogen in relevant quantities were only observed on Pt. The peak height is directly proportional to the applied voltage, and at 230 V, dissociation occurs. Hydrogen was observed on W and Pt. All spectra are normalized by the OH radical signal, the right side of the H_α line in (b) is cut off by a sensitivity gap in the echelle spectrometer.

rates (see below). Plasma−catalysis studies have shown that plasma-only N_2/H_2 chemistry typically favors NH_3 formation under nitrogen-rich conditions, whereas hydrogen-rich plasmas suppress NH_3 formation unless a catalytically active surface is present to stabilize and hydrogenate NH_x intermediates.[33] For both metals, we observe two distinctive plasma states, depending on the applied potential. The "cold" plasma, akin to a glow discharge, exhibits a characteristic neutral gas temperature (inferred from the rotational temperature of plasma-produced excited states i.e. the N_2(C−B) transition), ranging from 1000 to 1600 K. Notably, for this "cold" plasma state, we observe already a substantial amount of excited molecular nitrogen emission for the Pt cathode, but lower contributions from the W electrode (Figure 2a). For the "hot" plasma, resembling a hot discharge, the gas temperatures exceed 3000 K. (See the Methods section for the determination of the neutral gas temperature in the plasma).

The temperature of the active plasma electrode (cathode) could be determined by background continuum fitting and showed an applied potential dependency. When 175 V were applied, the temperature of the Pt wire is close to room temperature. Increasing the applied voltage to 200 V leads to temperatures around 900 K for the "cold" state and 1300 K for the "hot" state. Lastly, for the highest ammonia formation at 230 V, the electrode is at 1600 K, where it starts to become unstable and ultimately melts after a few minutes. The electrode temperatures on W are similar at the respective applied voltages, though no "cold" states could be observed.

For the Pt cathode, transitioning from the "cold" to the "hot" state significantly amplifies the N_2 (C−B, v' = 0−0) (vibrational state transitions between the $C^3\Pi_u$ and the B^3_g electronic states) peak intensities as well as the H_α spectral line, as shown in Figure 2a. Conversely, the ammonia production nearly quadruples for the hot plasma at around 200 V, suggesting energy-driven substantial dissociation of nitrogen. This observation supports our hypothesis that thermal water decomposition, occurring at electrode temperatures approaching 1000−1400 K on Pt[34], provides the necessary hydrogen radicals to stabilize the NH intermediate, thereby driving the formation of ammonia. However, the present data set does not isolate whether the dominant contribution is discharge-driven, thermally assisted water chemistry, hydrogen availability, or surface-mediated stabilization of NH_x intermediates. When investigating the potential dependence for the Pt cathode, we observe that at lower potential (180−200 V) the stronger emission from excited N_2 molecules is observed. At 230 V, the N_2 emission decreases again as seen in Figure 2b. The behavior for Pt is in clear contrast to that of W, for which we only detect sharp metallic lines, which are indicative of a higher surface heating level in the "hot" plasma state, but not of ammonia formation. This behavior is consistent with plasma-only chemistry under hydrogen-rich conditions, where NH_3 formation is suppressed in the absence of a catalytically active surface.

Taken together, the results in Figure 2 indicate that the interaction between the plasma and the cathode material influences NH_3 production beyond the effects of gas temperature, electron density, or H_2 generation alone. For example, under similar plasma parameters, Pt yields up to 7× higher NH_3 than W. This indicates a contribution from plasma-catalyst coupling. Depending on plasma parameters (hot vs cold plasma and applied bias), the discharge transitions from regimes of strong excited molecular N_2 emission to regimes of mainly atomic emission, which indicate substantial changes in the overall plasma chemistry and excitation dynamics. How these species subsequently contribute to NH_3 formation depends on the electrode material and its interaction with the plasma. Additionally, Pt possesses fast HER kinetics, which may influence the local hydrogen environment, but hydrogen generation alone does not explain the observed material dependence. A comparison between all materials at 10 and 200 V can be found in Supplementary Figure 2. Optical emission spectroscopy (Figure 2) shows that in the "hot" plasma state, vibrationally and electronically excited N_2 species are replaced by (fast quenched) atomic lines from the electrode material, as the electron densities increase and the electrode temperature rises. Furthermore, we note that the production rate of ammonia cannot be simply explained by changes in the gas temperature or electron density of the plasma, or H_2 production alone (see Supplementary Note 2), supporting our hypothesis of a real hybrid catalysis-plasma effect. At similar electron densities and neutral gas temperatures in the plasma, the production of NH_3 is far superior on Pt as compared to W.

Catalytic Properties and Parameter Space

The ammonia produced could be quantified reliably using the indophenol blue method,[10,35] due to the fact that substantially larger amounts of NH_3 generated as compared to the electrocatalytic NRR, which is prone to misinterpretation of NH_3 trace amounts.[10] Compared to eNRR, the NH_3

https://doi.org/10.1021/acsenergylett.5c01740
ACS Energy Lett. 2026, 11, 378−388

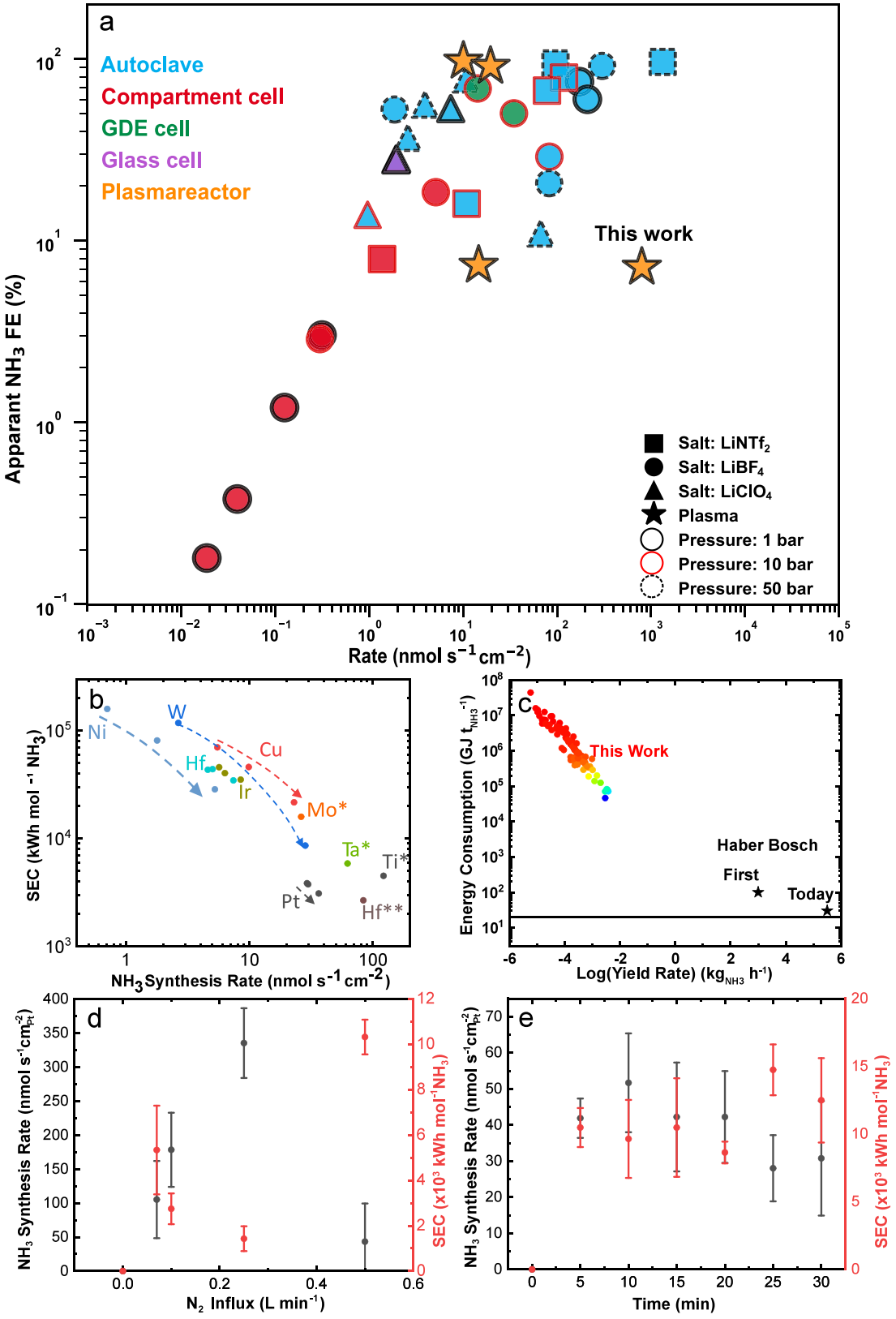

Figure 3. Apparent faradaic efficiency, specific energy consumption and NH_3 synthesis rate. (a) Comparison of results from various Li-mediated NRR studies to the findings of this work in terms of apparent faradaic efficiency and ammonia production rate (figure based on ref[37] see Supplementary Note 4) (b) Specific energy consumption vs NH_3 Synthesis rate measured with 0.07 L min^{-1} of N_2 flow and 200 V plasma voltage. Three successive measurements were performed for each material, with arrows in (b) indicating changes for the same wire between successive experiments. A general deactivation with each consecutive measurement was observed for the stable materials. Pt had the best reproducibility and was used as the standard for the following measurements. (c) Comparison of performance metrics to industrial Haber-Bosch thermal catalysis process in terms of energy consumption. The color coding represents the apparent faradaic efficiency from 0% (red) to 8% (blue) over all

https://doi.org/10.1021/acsenergylett.5c01740
ACS Energy Lett. 2026, 11, 378−388

Figure 3. continued

experiments. (d, e) NH_3 synthesis rate and specific energy consumption with N_2 inflow, and time, respectively. Materials labeled with "*" are deemed unstable due to fast dissolution of the cathode, while "**" denotes an initially inefficient but stable catalyst (e.g., Hf) after the natural passivation layer has worn off, and subsequently becoming unstable. If not stated otherwise, the measurements were conducted at 200 V bias, 0.07 L min^{-1} of N_2 inflow on a Pt cathode with 5 min of plasma.

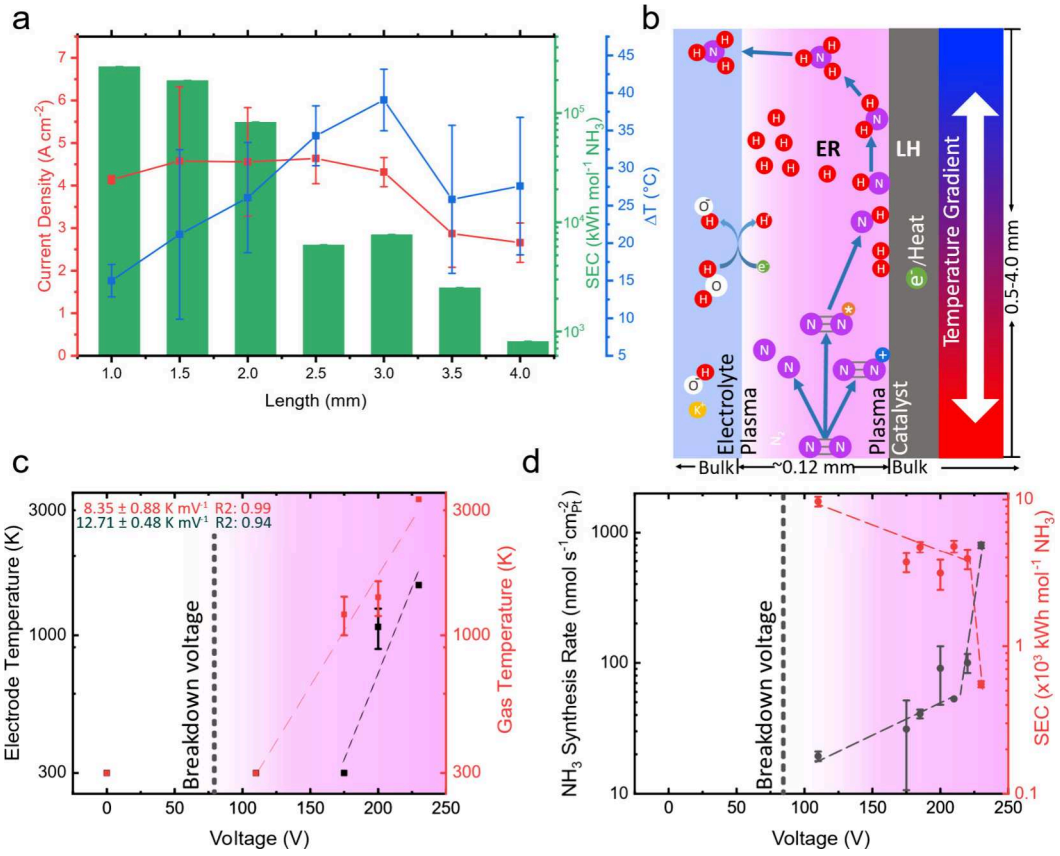

Figure 4. Impact of wire length on current density, temperature increase and specific energy consumption. (a) Relationship between the wire length of the active plasma electrode, increase of the electrolyte temperature during the experiment (blue), the current density (red), and the corresponding specific energy consumption (green). Between wire lengths of 3.0 mm and 3.5 mm, a transition can be observed, where the FE% drastically increases. (b) Schematic of the interface and possible mechanistic pathways for the hydrogenation of nitrogen species, starting from N_2*, N_2^+, NH, and atomic N. (c) Electrode and neutral gas temperatures as determined by blackbody continuum fit and the N_2(C−B) intensity. (d) Increase of FE(%) and production rate for ammonia depending on the applied voltage. The dotted line is a guide for the eye here.

production rate and current densities are here already superior, with only the apparent faradaic efficiency partially behind (Figure 3a), caused by the current required for the plasma.

The NH_3 generation rate is benchmarked against two categories: (i) plasma−water NRR systems, including gliding arc discharges,[25] plasma−over-liquid (micro)discharges,[27,28,31] and hybrid plasma−electrolysis cells;[32] and (ii) Li-mediated NRR systems, exemplified by the highly reliable and reproducible data set of Andersen et al.[10,36] The latter, while operating under a different mechanistic regime, serves as a trustworthy state-of-the-art reference due to rigorous control of the lack of ammonia detection due to contamination through a careful isotopic validation. This dual comparison enables both mechanistic context and performance benchmarking.

Figure 3b shows that Pt produces higher ammonia yields than W under otherwise identical plasma conditions. Corresponding OES spectra (Figure 2, Supplementary Figure 14) reveal differences in both N_2* and H* emission, which may arise from variations in plasma properties due to the electrode's electrical characteristics. While these spectral differences could suggest different extents of plasma-driven activation, the present data do not isolate possible catalytic surface effects from changes in discharge characteristics. Notably, materials such as Cu, Ni, and W exhibited significant reduction in synthesis rate and higher specific energy consumption (SEC) with each consecutive measurement (despite stable plasma conditions ranging from 5 min up to 1 h), while Pt, Hf, and Ir demonstrated greater stability. Despite their high activity, electrodes made of Ta and Ti endured only a few seconds under plasma conditions before their complete dissolution into the electrolyte. Hf, distinguished by its natural inert oxide layer, exhibited behavior akin to Ir. However, once the protective layer was compromised (indicated by the Hf** in Figure 3b), it mirrored the rapid degradation observed for Ti and Ta. As mentioned above, Pt is the best-performing and simultaneously the most plasma resistant material among those tested here, likely due to the combined plasma and catalytic properties that are needed for high NH_3 synthesis rates. Supplementary Figures 3−6 display the XPS measurements on Cu, W, and Pt acquired before and

https://doi.org/10.1021/acsenergylett.5c01740
ACS Energy Lett. 2026, 11, 378−388

after plasma operation. While reoxidation in air is a possibility (especially for Cu), an increase of oxide compared to the pristine state indicates changes originating from the experiment.

Figure 3c compares the specific (electrical) energy consumption for ammonia production in our system to the optimized industrial Haber−Bosch process.[1] This benchmark represents large-scale thermal catalysis under >400 °C and >200 atm conditions and is included here solely to contextualize energy efficiency. The comparison does not imply that the present proof of concept system is competitive with industrial Haber−Bosch at its current scale. Noteworthy, even small changes in the system, e.g. exact plasma potential, can lead to dramatic changes and improvements. See Supplementary Note 3 for a discussion on the thermodynamics. Figure 3d shows that increasing the N_2 inflow is beneficial up to a certain threshold, beyond which it disrupts the formation of the gas sheath. Figure 3e shows the NH_3 production over time, with aliquots taken every 5 min with a continuous "hot" plasma state for 30 min and 0.07 L min^{-1} of nitrogen inflow.

Taken together, the results in Figure 3 clearly show that the Pt plasma cathode leads to the highest ammonia production among all tested materials, with almost 2 orders of magnitude higher yields compared to W. Furthermore, doubling the N_2 flow leads to almost double the amount of NH_3 produced, which strongly indicates that the exact flow and plasma conditions, which are not yet optimized in this proof of concept study, are critical for a high NH_3 rate, and that there is a great potential for improved yields with new reactor designs. In particular, we hypothesized that a larger exposed plasma area on the Pt wire should lead to increased yields.

Wire Length and Plasma Correlation

To assess the effect of the exposed wire surface, we systematically varied the length of the plasma cathode wire in our reactor 1.0 mm to 4.0 mm. Here, the parameter varied is the protrusion of the wire into the electrolyte and hence into the plasma-forming gas/vapor sheath. As the protrusion increases, both the plasma-active surface and the sheath hydrodynamics change, leading to nonlinear behavior in FE and production rate. The pronounced increase in FE from 3.5 to 4.0 mm is consistent with a threshold in sheath stability and hot-discharge persistence near the tip, rather than linear geometric scaling (Figure 4a). For wire lengths >3 mm, a substantial enhancement in faradaic efficiency is observed, paralleled by a drop in current density and a 40% reduction of the temperature change at 4 mm. We ascribe this behavior to the formation of a stable contact glow discharge (CGDC) plasma, a condition hindered by the emergence of bubbles from the N_2 inlet at smaller wire lengths. We observed that increasing the plasma wire length not only enhances the specific energy consumption but also creates spatial regions with distinct thermal profiles. The longer wire exposes a larger area to the hot plasma conditions required for water decomposition, thereby generating abundant hydrogen radicals. Simultaneously, cooler regions along the wire allow the Pt surface to effectively bind and hydrogenate activated nitrogen species, culminating in a robust and synergistic pathway for ammonia synthesis. The reduction in current density (at constant potential of 200 V) and temperature increase over the 5 min of reaction is attributed to the increased resistance at the interface, stemming from the presence of the gas sheath. Moreover, the transition of liquid water to vapor during the process reduces the energy requirement for water electrolysis and thermal decomposition, increasing thus the available hydrogen for ammonia formation. In the plasma, the generation of ions and radicals might enable a nonthermal Eley−Rideal (ER) reaction mechanism alongside the thermal Langmuir−Hinshelwood (LH) mechanism. Short-lived atomic nitrogen species produced in the plasma stabilize upon adsorption onto the cathode surface, particularly favored by Pt, which exhibits strong nitrogen binding. Possibly following a reverse Gerischer−Mauerer mechanism,[38] the Pt surface can bind nitrogen, and partially hydrated intermediates, which eventually form ammonia that might detach in the cooler regions of the cathode. A crucial intermediate seems to be the NH radical. Partial hydration or direct reaction with hydrogen are possible. ER/LH pathways on the catalyst surface are the main contributors here. The discussion of possible (LH) and (ER) pathways is presented here as a working hypothesis informed by the reactor geometry and OES observations, rather than as a definitive mechanistic assignment. Concurrently, electrode temperatures of 900−1600 K (Figure 4c) approach those reported for catalytic thermal decomposition of water,[34] producing H radicals. These radicals can combine with plasma-activated nitrogen species at or near the Pt surface, stabilizing NH intermediates. Such coupling of plasma excitation and surface catalysis has been described for related N_2 plasma systems,[38,39] supporting the proposed Langmuir−Hinshelwood/Eley−Rideal pathways here. Additionally, from the N_2(C−B) transition, the neutral gas temperature could be determined. This increase in temperature correlates well with the sudden decrease in specific energy consumption (Figure 4d). The high densities of $H^{\bullet}$ radicals (and potential $N^{\bullet}$ radicals) suggest an ER-type contribution, where reactive radicals impinge directly on the hot electrode surface.[23,29,40,41] LH-type contributions could occur if adsorbed N and H species recombine on cooler sections of the submerged electrode or at sheath boundaries where radicals are quenched.[42,43] Distinguishing their relative contributions will require targeted operando and isotopic-labeling studies, which are planned for future work. When materials other than Pt were used as cathode, lower or negligible ammonia yields were observed. However, in our reactor configuration, where plasma forms directly around the submerged cathode tip in a nitrogen-fed gas/vapor sheath, the stability of the cathode material is critical for maintaining a consistent plasma regime. Many materials tested (Ti, Ta, Mo) dissolved in the electrolyte, while Cu and Ni rapidly lost electrical contact due to surface degradation, and Hf showed similar instability. Only Pt, W, and Ir maintained structural integrity, though Ir and W exhibited lower activity. This suggests that both cathode stability and plasma-surface interaction properties contribute to sustained ammonia production, and that low yields from unstable materials cannot be attributed solely to the absence of heterogeneous catalytic effects. This process is schematically depicted in Figure 4b and summarized in Supplementary Note 5. In our configuration, plasma forms directly around the submerged wire tip within a nitrogen-fed gas/vapor sheath. The temperatures in Figure 4a represent average bulk electrolyte temperature values and do not capture potential local variations along the protruding segment. The observed FE increase from 3.5 to 4.0 mm, despite similar measured temperatures, indicates that sheath stability, gas residence time, and reactive species density may play a more important role

https://doi.org/10.1021/acsenergylett.5c01740
ACS Energy Lett. 2026, 11, 378−388

than bulk temperature alone. Supplementary Note 2 contains high-speed camera measurements of the stochastic discharge distribution, corroborating this hypothesis of an inhomogeneous plasma distribution. Figure 4c shows the increase of temperature of the electrode and the bulk gas temperature. Figure 4d shows the specific energy consumption and NH_3 synthesis rate (log scale) in relation to the applied voltage used to generate the plasma. In the voltage range between the minimum threshold required for plasma ignition (80 V) and the onset of the hot plasma state (first observed at 200 V), only small amounts of ammonia are detected with Pt. However, as the potential reaches the range where the hot state becomes predominant (230 V), the efficiency of ammonia synthesis spikes dramatically. At even higher potentials the cathode and/or the gas sheath become unstable, likely due to excessive heating.

To probe any remaining species on the electrode surface, cyclic voltammetry was conducted immediately after 5 min of plasma. The surface of the electrode becomes roughened, which can be seen from the pseudocapacitive increase of the CVs of about a factor of 3. Additionally, it can be observed that the hydrogen adsorption/desorption regime is shifted down due to the presence of oxygen. A new peak appears at 0.5 V_{RHE} during the first CV cycle but disappears in subsequent scans. This feature is consistent with the onset of the ammonia oxidation reaction (AOR), and does not appear when Ar is used instead of N_2 for the feed gas. This could be the onset of the ammonia oxidation reaction (AOR), which disappears once the adsorbed ammonia is fully oxidized. A clear distinction between Pt oxidation and AOR around 0.9 V_{RHE} is not possible. A shoulder peak at 0.7 to 0.8 V_{RHE} is associated with Pt-hydroxide formation and gets more pronounced with the exposure to hydroxyl radicals during plasma. Directly after the plasma, the Pt−O reduction peak at 0.57 V_{RHE} increases and the H_{upd} adsoption and desorption become more pronounced, as seen in Figure 5a,b. Ex-situ postreaction XPS analysis (Figure 5c) shows no distinct surface compositional changes, including Pt oxidation and the presence of adventitious nitrogen species or potassium (from KOH) on the cathode surface. These data, obtained after plasma operation, indicate that the electrode undergoes no chemical modification during operation, which may influence plasma−surface interactions. Surface changes were observed after plasma operation via scanning electron microscopy. The loss of material was tracked via ICP-MS (Supplementary Figure 8). For Pt, no visible structural damage occurred, and XPS spectra showed only minor oxidation. In contrast, Ti, Ta, and Mo exhibited clear signs of corrosion and pitting after ≤10 min of operation. These findings confirm that electrolyte contact at the electrode tip can lead to significant degradation for certain metals, likely affecting the plasma's stability and NH_3 production.

In conclusion, we have carried out proof-of-concept experiments and demonstrated the ability of generating NH_3 from N_2 with an in-liquid plasma-catalytic reactor. Among the tested electrode materials, platinum exhibited optimal stability and catalytic conversion, in clear contrast to W, which also formed a stable plasma, but produced only minor amounts of NH_3. The attainment of the hot plasma state at potentials exceeding 200 V resulted in a 4-fold improvement in specific energy consumption for ammonia compared to the cold plasma state. The optimal nitrogen flow was observed at 0.07 L min^{-1}, striking a balance between plasma gas sheath stability

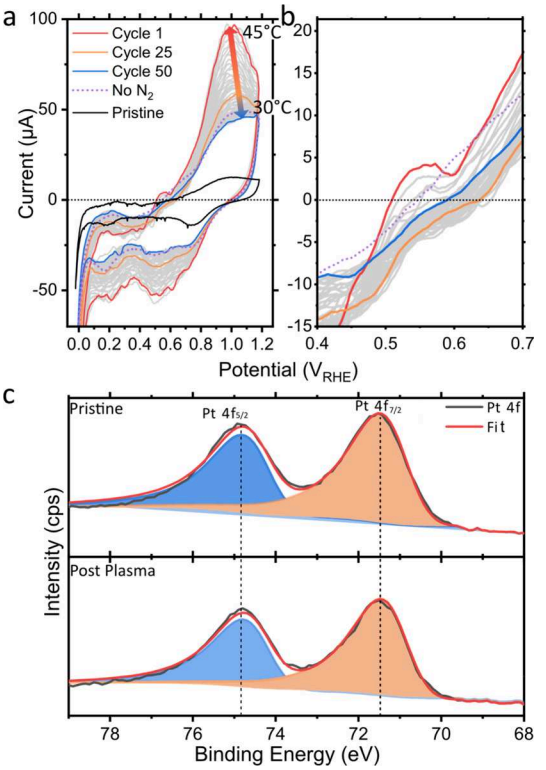

Figure 5. Cyclic voltammetry and ex-situ XPS data before and after plasma. (a) Cyclic voltammetry on a fresh 3.0 mm Pt wire before (black) and after plasma (blue to red). The first 50 cycles after plasma were collected between 45 °C and 30 °C (constant cooling). The dotted purple line indicates a measurement without N_2. (b) is a zoom in the AOR region. All CVs were collected at 50 mV s^{-1} in 0.1 M KOH and 0.07 L min^{-1} of N_2 inflow around the electrode. (c) Ex-situ XPS data of the Pt 4f region before and after plasma.

and activity. While the system demonstrated stability over 30 min, the operation conditions are not yet fully optimized, and challenges persisted in preventing the potential outgassing or thermal decomposition of the formed ammonia, even with intermittent cooling intervals every 5 min. Addressing this issue necessitates an improved solution for ammonia collection or an enhanced cooling mechanism. Distinct hot and cold states resembling those reported in established plasma systems such as hot and cold discharge were monitored via optical emission spectroscopy. In the hot discharge state, molecular excited nitrogen species were absent, with nitrogen undergoing atomic splitting and recombination with hydrogen from water splitting at temperatures exceeding 3000 K. We propose also a reaction pathway from a combination of Gerischer-Maurer mechanism to bind atomic nitrogen to the catalyst surface followed by Langmuir−Hinshelwood and Eley−Rideal mechanisms to form ammonia. Our findings collectively contribute to the understanding of plasma-catalyzed nitrogen reduction in liquid environments, laying the foundation for further advancements in this field.

The presented system is still in its early development, and the full understanding of the intriguing findings observed will require more in-depth insight into the thermal catalysis, electrochemical catalysis and plasma catalysis processes involved. In addition, further optimization of the reactor configuration and electrode parameters should be undertaken in order to enhance the currently low energy efficiency. The first attempts were illustrated here, including varying the

https://doi.org/10.1021/acsenergylett.5c01740
ACS Energy Lett. 2026, 11, 378−388

plasma wire length, the plasma electrode geometries and materials as well as implementing a new reactor design with improved N_2 gas flow.

Finally, beyond NH_3 production, we envision that such a plasma-catalytic reactor might also be used to attain high rate CO_2 reduction and other critical chemical energy conversions, especially when green electricity is cheap and abundant and a high conversion rate is needed.

■ ASSOCIATED CONTENT

Supporting Information

The Supporting Information is available free of charge at https://pubs.acs.org/doi/10.1021/acsenergylett.5c01740.

Additional experimental details, materials, and methods; Supplementary Notes 1−7: electrochemical/plasma diagnostics, plasma-parameter estimates, thermodynamic calculations, literature comparison, mechanistic discussion, and performance/calibration calculations; Supplementary Tables 1−6: E/N and electron densities, N_2 rotational temperature, thermochemistry, literature data set for Figure 3a, mechanistic steps, XPS fit parameters; Supplementary Figures 1−24: reactor schematics, electrochemical/plasma diagnostics incl. SPEIS, I−V, OES/imaging, XPS/ICP-MS, thermodynamic/energy analyses (PDF)

■ AUTHOR INFORMATION

Corresponding Authors

Philipp Grosse − *Department of Interface Science, Fritz-Haber Institute of the Max Planck Society, 14195 Berlin, Germany;* orcid.org/0000-0003-0738-250X; Email: grosspk7@fhi-berlin.mpg.de

Beatriz Roldan Cuenya − *Department of Interface Science, Fritz-Haber Institute of the Max Planck Society, 14195 Berlin, Germany;* orcid.org/0000-0002-8025-307X; Email: roldan@fhi-berlin.mpg.de

Authors

Jan-Luca Gembus − *Chair of Applied Electrodynamics and Plasma Technology, Ruhr University Bochum, 44801 Bochum, Germany*

Felix Landwehr − *Department of Interface Science, Fritz-Haber Institute of the Max Planck Society, 14195 Berlin, Germany;* orcid.org/0000-0001-7653-3311

Alex Ricardo Silva Olaya − *Department of Interface Science, Fritz-Haber Institute of the Max Planck Society, 14195 Berlin, Germany;* orcid.org/0000-0003-2915-6618

Daniel Escalera-López − *Department of Interface Science, Fritz-Haber Institute of the Max Planck Society, 14195 Berlin, Germany;* orcid.org/0000-0002-2001-9775

Nikita Bibinov − *Chair of Applied Electrodynamics and Plasma Technology, Ruhr University Bochum, 44801 Bochum, Germany*

Andrew Robert Gibson − *Chair of Applied Electrodynamics and Plasma Technology, Ruhr University Bochum, 44801 Bochum, Germany; York Plasma Institute, School of Physics, Engineering and Technology, University of York, Heslington YO10 5DD, United Kingdom*

Sebastian Zeki Oener − *Department of Interface Science, Fritz-Haber Institute of the Max Planck Society, 14195 Berlin, Germany;* orcid.org/0000-0003-0770-4089

Complete contact information is available at: https://pubs.acs.org/10.1021/acsenergylett.5c01740

Author Contributions

P.G., S.Z.O., and B.R.C. conceived of the project and planned the experiments. P.G. built the reactor and conducted the experiments. P.G., J.L.G., N.B., and A.R.G. conducted and analyzed the spectroscopic plasma experiments. D.E.L. conducted the ICP-MS experiments. A.R.O.S. and P.G. conducted and analyzed the GC measurements. P.G., S.Z.O., N.B., and J.L.G. analyzed and interpreted the data. P.G., S.Z.O., and B.R.C. wrote the manuscript with input from all authors.

Funding

Open access funded by Max Planck Society.

Notes

The authors declare no competing financial interest.

■ ACKNOWLEDGMENTS

We acknowledge funding by the Deutsche Forschungsgemeinschaft (DFG, German Research Foundation) − project no. 327886311 − SFB 1316, subproject B1 and B5. We also appreciate the insightful discussions with Prof. Robert Schlögl.

■ REFERENCES

(1) Humphreys, J.; Lan, R.; Tao, S. Development and recent progress on ammonia synthesis catalysts for Haber−Bosch process. *Adv. Energy Sustain. Res.* **2021**, *2* (1), 2000043.

(2) Kyriakou, V.; Garagounis, I.; Vourros, A.; Vasileiou, E.; Stoukides, M. J. J. An electrochemical haber-bosch process. *Joule* **2020**, *4* (1), 142−158.

(3) MacFarlane, D. R.; Cherepanov, P. V.; Choi, J.; Suryanto, B. H.R.; Hodgetts, R. Y.; Bakker, J. M.; Ferrero Vallana, F. M.; Simonov, A. N. A roadmap to the ammonia economy. *Joule* **2020**, *4* (6), 1186−1205.

(4) Smith, C.; Hill, A. K.; Torrente-Murciano, L. Current and future role of Haber−Bosch ammonia in a carbon-free. *Energy Landscape* **2020**, *13* (2), 331−344.

(5) Wang, M.; Khan, M. A.; Mohsin, I.; Wicks, J.; Ip, A. H.; Sumon, K. Z.; Dinh, C.-T.; Sargent, E. H.; Gates, I. D.; Kibria, M. G. Can sustainable ammonia synthesis pathways compete with fossil-fuel based Haber−Bosch processes? *Energy Environ. Sci.* **2021**, *14* (5), 2535−2548.

(6) Li, K.; Andersen, S. Z.; Statt, M. J.; Saccoccio, M.; Bukas, V. J.; Krempl, K.; Sažinas, R.; Pedersen, J. B.; Shadravan, V.; Zhou, Y.; Chakraborty, D.; Kibsgaard, J.; Vesborg, P. C. K.; Nørskov, J. K.; Chorkendorff, I. Enhancement of lithium-mediated ammonia synthesis by addition of oxygen. *Science* **2021**, *374* (6575), 1593−1597.

(7) Fu, X.; Pedersen, J. B.; Zhou, Y.; Saccoccio, M.; Li, S.; Sažinas, R.; Li, K.; Andersen, S. Z.; Xu, A.; Deissler, N. H.; Mygind, J. B. V.; Wei, C.; Kibsgaard, J.; Vesborg, P. C. K.; Nørskov, J. K.; Chorkendorff, I. Continuous-flow electrosynthesis of ammonia by nitrogen reduction and hydrogen oxidation. *Science* **2023**, *379* (6633), 707−712.

(8) Mushtaq, M. A.; Arif, M.; Yasin, G.; Tabish, M.; Kumar, A.; Ibraheem, S.; Ye, W.; Ajmal, S.; Zhao, J.; Li, P. J. R.; Reviews, S. E.; et al. Recent developments in heterogeneous electrocatalysts for ambient nitrogen reduction to ammonia: Activity, challenges, and future perspectives. *Renew. Sustain. Energy Rev.* **2023**, *176*, 113197.

(9) Fichter, F.; Girard, P.; Erlenmeyer, H. J. H. C. A. Elektrolytische Bindung von komprimiertem Stickstoff bei gewöhnlicher Temperatur. *Ann. Phys.* **1930**, *13* (6), 1228−1236.

(10) Andersen, S. Z.; Čolić, V.; Yang, S.; Schwalbe, J. A.; Nielander, A. C.; McEnaney, J. M.; Enemark-Rasmussen, K.; Baker, J. G.; Singh, A. R.; Rohr, B. A. J. N.; et al. A rigorous electrochemical ammonia

synthesis protocol with quantitative isotope measurements. *Nature* **2019**, *570* (7762), 504−508.
(11) Nielander, A. C.; McEnaney, J. M.; Schwalbe, J. A.; Baker, J. G.; Blair, S. J.; Wang, L.; Pelton, J. G.; Andersen, S. Z.; Enemark-Rasmussen, K.; Colic, V. J. A. C.; et al. A versatile method for ammonia detection in a range of relevant electrolytes via direct nuclear magnetic resonance techniques. *ACS Catal.* **2019**, *9* (7), 5797−5802.
(12) Suryanto, B. H. R.; Matuszek, K.; Choi, J.; Hodgetts, R. Y.; Du, H.-L.; Bakker, J. M.; Kang, C. S. M.; Cherepanov, P. V.; Simonov, A. N.; MacFarlane, D. R. Nitrogen reduction to ammonia at high efficiency and rates based on a phosphonium proton shuttle. *Science* **2021**, *372* (6547), 1187−1191.
(13) Li, S.; Zhou, Y.; Fu, X.; Pedersen, J. B.; Saccoccio, M.; Andersen, S. Z.; Enemark-Rasmussen, K.; Kempen, P. J.; Damsgaard, C. D.; Xu, A.; Sažinas, R.; Mygind, J. B. V.; Deissler, N. H.; Kibsgaard, J.; Vesborg, P. C. K.; Nørskov, J. K.; Chorkendorff, I. Long-term continuous ammonia electrosynthesis. *Nature* **2024**, *629* (8010), 92−97.
(14) Liang, J.; Li, Z.; Zhang, L.; He, X.; Luo, Y.; Zheng, D.; Wang, Y.; Li, T.; Yan, H.; Ying, B.; Sun, S.; Liu, Q.; Hamdy, M. S.; Tang, B.; Sun, X. Advances in ammonia electrosynthesis from ambient nitrate/nitrite reduction. *Chem.* **2023**, *9* (7), 1768−1827.
(15) Bai, L.; Franco, F.; Timoshenko, J.; Rettenmaier, C.; Scholten, F.; Jeon, H. S.; Yoon, A.; Rüscher, M.; Herzog, A.; Haase, F. T.; Kühl, S.; Chee, S. W.; Bergmann, A.; Beatriz, R. C. Electrocatalytic Nitrate and Nitrite Reduction toward Ammonia Using Cu2O Nanocubes: Active Species and Reaction Mechanisms. *J. Am. Chem. Soc.* **2024**, *146* (14), 9665−9678.
(16) Yoon, A.; Bai, L.; Yang, F.; Franco, F.; Zhan, C.; Rüscher, M.; Timoshenko, J.; Pratsch, C.; Werner, S.; Jeon, H. S.; Monteiro, M. C. d. O.; Chee, S. W.; Roldan Cuenya, B. Revealing catalyst restructuring and composition during nitrate electroreduction through correlated operando microscopy and spectroscopy. *Nat. Mater.* **2025**, *24* (5), 762−769.
(17) Liu, H.; Lang, X.; Zhu, C.; Timoshenko, J.; Rüscher, M.; Bai, L.; Guijarro, N.; Yin, H.; Peng, Y.; Li, J.; Liu, Z.; Wang, W.; Cuenya, B. R.; Luo, J. Efficient Electrochemical Nitrate Reduction to Ammonia with Copper-Supported Rhodium Cluster and Single-Atom. *Catalysts* **2022**, *61* (23), e202202556.
(18) Zhang, K.; Cao, A.; Wandall, L. H.; Vernieres, J.; Kibsgaard, J.; Nørskov, J. K.; Chorkendorff, I. Spin-mediated promotion of Co catalysts for ammonia synthesis. *Science* **2024**, *383* (6689), 1357−1363.
(19) Cao, A.; Bukas, V. J.; Shadravan, V.; Wang, Z.; Li, H.; Kibsgaard, J.; Chorkendorff, I.; Nørskov, J. K. A spin promotion effect in catalytic ammonia synthesis. *Nat. Commun.* **2022**, *13* (1), 2382.
(20) Ma, H.; Schneider, W. F. J. A. C. Structure-and temperature-dependence of Pt-catalyzed ammonia oxidation rates and selectivities. *ACS Catal.* **2019**, *9* (3), 2407−2414.
(21) Breneman, A. A. The fixation of atmospheric nitrogen. *J. Am. Chem. Soc.* **1889**, *11* (2), 31−48.
(22) Wang, W.; Patil, B.; Heijkers, S.; Hessel, V.; Bogaerts, A. J. C. Nitrogen fixation by gliding arc plasma: better insight by chemical kinetics modelling. *ChemSusChem* **2017**, *10* (10), 2145−2157.
(23) Zhang, T.; Zhou, R.; Zhang, S.; Zhou, R.; Ding, J.; Li, F.; Hong, J.; Dou, L.; Shao, T.; Murphy, A. B.; Ostrikov, K.; Cullen, P. J. Sustainable Ammonia Synthesis from Nitrogen and Water by One-Step Plasma Catalysis. *Energy & Environmental Materials* **2023**, *6* (2), e12344.
(24) Yang, X.; Zhang, Y.; Liao, H.; Tian, C.; Cui, J.; Liu, Z. Nitrogen Fixation via Catalyst-Free Water-Falling Film Dielectric Barrier Discharge Plasma: A Novel and Simple Strategy to Enhance Ammonia Selectivity. *Applied Sciences* **2025**, *15* (3), 1410.
(25) Indumathy, B.; Ananthanarasimhan, J.; Rao, L.; Yugeswaran, S.; Ananthapadmanabhan, P. V. Catalyst-free production of ammonia by means of interaction between a gliding arc plasma and water surface. *J. Phys. D: Appl. Phys.* **2022**, *55* (39), 395501.
(26) Yoshida, S.; Murakami, N.; Takatsuji, Y.; Haruyama, T. Elucidation of the behavior of oxygen remaining in water molecules after hydrogen atom abstraction in the plasma/liquid (P/L) interfacial reaction: improvement in the selectivity of ammonia synthesis and parallel production of hydrogen gas. *Green Chem.* **2023**, *25* (2), 579−588.
(27) Sharma, R. K.; Patel, H.; Mushtaq, U.; Kyriakou, V.; Zafeiropoulos, G.; Peeters, F.; Welzel, S.; van de Sanden, M. C. M.; Tsampas, M. N. Plasma Activated Electrochemical Ammonia Synthesis from Nitrogen and Water. *ACS Energy Letters* **2021**, *6* (2), 313−319.
(28) Hawtof, R.; Ghosh, S.; Guarr, E.; Xu, C.; Mohan Sankaran, R.; Renner, J. N. Catalyst-free, highly selective synthesis of ammonia from nitrogen and water by a plasma electrolytic system. *Science Advances* **2019**, *5* (1), eaat5778.
(29) Hong, J.; Zhang, T.; Zhou, R.; Dou, L.; Zhang, S.; Zhou, R.; Ashford, B.; Shao, T.; Murphy, A. B.; Ostrikov, K.; Cullen, P. J. Green chemical pathway of plasma synthesis of ammonia from nitrogen and water: a comparative kinetic study with a N2/H2 system. *Green Chem.* **2022**, *24* (19), 7458−7468.
(30) Huang, J.; Qu, Z.; Gao, Y.; Fan, J.; Gan, D.; Sun, J.; Li, T.; Zhang, T.; Cullen, P. J.; Zhou, R. Sustainable liquid nitrogen fertilizer production via air plasma bubbles: insights into plasma-enabled N2 fixation chemistry. *J. Phys. D: Appl. Phys.* **2025**, *58* (11), 115207.
(31) Lamichhane, P.; Paneru, R.; Nguyen, L. N.; Lim, J. S.; Bhartiya, P.; Adhikari, B. C.; Mumtaz, S.; Choi, E. H. Plasma-assisted nitrogen fixation in water with various metals. *Reaction Chemistry & Engineering* **2020**, *5* (11), 2053−2057.
(32) Sun, J.; Alam, D.; Daiyan, R.; Masood, H.; Zhang, T.; Zhou, R.; Cullen, P. J.; Lovell, E. C.; Jalili, A.; Amal, R. A hybrid plasma electrocatalytic process for sustainable ammonia production. *Energy Environ. Sci.* **2021**, *14* (2), 865−872.
(33) Mehta, P.; Barboun, P.; Go, D. B.; Hicks, J. C.; Schneider, W. F. Catalysis Enabled by Plasma Activation of Strong Chemical Bonds: A Review. *ACS Energy Letters* **2019**, *4* (5), 1115−1133.
(34) Jellinek, H. H. G.; Kachi, H. The catalytic thermal decomposition of water and the production of hydrogen. *Int. J. Hydrogen Energy* **1984**, *9* (8), 677−688.
(35) Bolleter, W.; Bushman, C.; Tidwell, P. W. J. A. C. Spectrophotometric determination of ammonia as indophenol. *Anal. Chem.* **1961**, *33* (4), 592−594.
(36) Andersen, S. Z.; Statt, M. J.; Bukas, V. J.; Shapel, S. G.; Pedersen, J. B.; Krempl, K.; Saccoccio, M.; Chakraborty, D.; Kibsgaard, J.; Vesborg, P. C. K.; Nørskov, J.; Chorkendorff, I. Increasing stability, efficiency, and fundamental understanding of lithium-mediated electrochemical nitrogen reduction. *Energy Environ. Sci.* **2020**, *13* (11), 4291−4300.
(37) Chang, W.; Jain, A.; Rezaie, F.; Manthiram, K. Lithium-mediated nitrogen reduction to ammonia via the catalytic solid−electrolyte interphase. *Nature Catalysis* **2024**, *7* (3), 231−241.
(38) Gerischer, H.; Mauerer, A. Untersuchungen Zur anodischen Oxidation von Ammoniak an Platin-Elektroden. *Journal of Electroanalytical Chemistry and Interfacial Electrochemistry* **1970**, *25* (3), 421−433.
(39) Tulenbergenov, T.; Skakov, M.; Kolodeshnikov, A.; Zuev, V.; Rakhadilov, B.; Sokolov, I.; Ganovichev, D.; Miniyazov, A.; Bukina, O. Interaction between nitrogen plasma and tungsten. *Nuclear Materials and Energy* **2017**, *13*, 63−67.
(40) Rouwenhorstm, K. H. R.; Lefferts, L. Plasma-catalytic Ammonia Synthesis via Eley-Rideal Reactions: A Kinetic Analysis. *ChemCatChem.* **2023**, *15* (12), No. e202300078.
(41) Hong, J.; Pancheshnyi, S.; Tam, E.; Lowke, J. J.; Prawer, S.; Murphy, A. B. Kinetic modelling of NH3 production in N2−H2 non-equilibrium atmospheric-pressure plasma catalysis. *J. Phys. D: Appl. Phys.* **2017**, *50* (15), 154005.
(42) Rodriguez, J. A.; Jirsak, T.; Liu, G.; Hrbek, J.; Dvorak, J.; Maiti, A. Chemistry of NO2 on Oxide Surfaces: Formation of NO3 on TiO2(110) and NO2↔O Vacancy Interactions. *J. Am. Chem. Soc.* **2001**, *123* (39), 9597−9605.

(43) Shah, J.; Wang, W.; Bogaerts, A.; Carreon, M. L. Ammonia Synthesis by Radio Frequency Plasma Catalysis: Revealing the Underlying Mechanisms. *ACS Applied Energy Materials* **2018**, *1* (9), 4824−4839.

https://doi.org/10.1021/acsenergylett.5c01740
ACS Energy Lett. 2026, 11, 378−388